Journal of Magnetism and Magnetic Materials 419 (2016) 517–520

Contents lists available at ScienceDirect

Journal of Magnetism and Magnetic Materials

journal homepage: www.elsevier.com/locate/jmmm

Coercivity scaling in antidot lattices in Fe, Ni, and NiFe thin films

Joachim Gräfe *, Gisela Schütz, Eberhard J. Goering **

Max Planck Institute for Intelligent Systems, Heisenbergstraße 3, 70569 Stuttgart, Germany

ARTICLE INFO

Article history:
Received 14 June 2016
Accepted 22 June 2016
Available online 23 June 2016

ABSTRACT

Antidot lattices can be used to artificially engineer magnetic properties in thin films, however, a conclusive model that describes the coercivity enhancement in this class of magnetic nano-structures has so far not been found. We prepared Fe, Ni, and NiFe thin films and patterned each with 21 square antidot lattices with different geometric parameters and measured their hysteretic behavior. On the basis of this extensive dataset we are able to provide a model that can describe both the coercivity scaling over a wide range of geometric lattice parameters and the influence of different materials.

1. Introduction

Periodic arrangements of nano-scaled holes, so-called antidot lattices, in magnetic thin films have been investigated in a wide scientific context and in different host materials. Various novel phenomena like artificial spin ice [1] and spin glass [2], and pairs of magnetic monopoles [3] have been reported in antidot lattices. They can be applied as spin wave guides and filters [4] or in the context of data storage as a type of bit patterned media, because antidot lattices can overcome the superparamagnetic limit as there are no isolated magnetic islands [5]. Furthermore, antidot lattices influence the magnetic properties of the host materials and can be used to tune the magnetic anisotropy [6–8] and coercivity [9–11]. Therefore, nano-scaled antidot lattices can be used to engineer application specific coercive field.

For application driven adjustment of the magnetic properties, however, a quantitative description of the geometric scaling of the coercivity in antidot lattices is desirable and has been sought for in several studies [12–19]. Modeling is based on pinning of domain walls at point defects [20]. Therefore, it is assumed that the defect size, *i.e.* the antidot diameter d, is larger than the width of the domain wall, and that the length of the domain wall is determined by the width w of the material bridge between two adjacent holes [12–19,21]. Following work on coercivity scaling in flat magnetic wires [22] a $1/w$ – dependency of the coercivity in antidot lattices is assumed [12–16]. Because flexible nanolithography approaches like e-beam or focused ion beam techniques have slow writing speeds, it is challenging to get sufficiently large samples for many measurement techniques and it is difficult to manufacture a large number of samples. Thus, previous studies relied on a very limited number of samples [12–17] and different magnetic materials were rarely compared [19,21]. Hence, the validity of a strict $1/w$ – dependency has so far been inconclusive [18]. Here, we present an extensive parametric study of antidot lattices in films of Fe, Ni, and NiFe and discuss modeling of their coercivities relying on a broader data base.

2. Methods

Therefore, 20 nm thin films of these materials were deposited by ion beam sputtering on Si(001) and capped by 2 nm Al. Subsequently, $20 \times 20\ \mu m^2$ antidot patterns with different lattice parameters were etched by a focused Ga^+ ion beam in a FEI Nova 600 NanoLab DualBeam with an Raith ELPHY Multibeam pattern generator. Such a set of 21 square antidot lattices with diameters d ranging from 25 to 525 nm and lattice constants a of 200, 400, and 600 nm are shown in Fig. 1. For each value of a seven lattices have been produced with linearly increasing d from $1/8 \cdot a$ to $7/8 \cdot a$. It has been shown by Castán-Guerrero et al. [17] that the coercivity and the magnetization reversal process are not changed by the antidot lattice being embedded in a continuous film or standing freely as isolated island.

Hysteresis loops of the individual antidot lattices were recorded using a Durham Magneto Optics NanoMOKE3 equipped with an air cooled vector electromagnet, capable of generating in-plane fields up to 120 mT. Measurements were conducted in longitudinal geometry and the laser beam was focussed with an aspheric lens ($f = 11$ mm) at an incidence angle of 45° onto the sample. This results in an imaging resolution of 1 μm and an area of smaller than $5 \times 5\ \mu m^2$ that contributes to the magnetic signal. An exemplary set of three hystereses of the pristine Fe thin film and two antidot lattices hosted in it is shown in Fig. 2 where the

* Corresponding author.
** Principal corresponding author.
E-mail addresses: graefe@is.mpg.de (J. Gräfe), goering@is.mpg.de (E.J. Goering).

http://dx.doi.org/10.1016/j.jmmm.2016.06.052

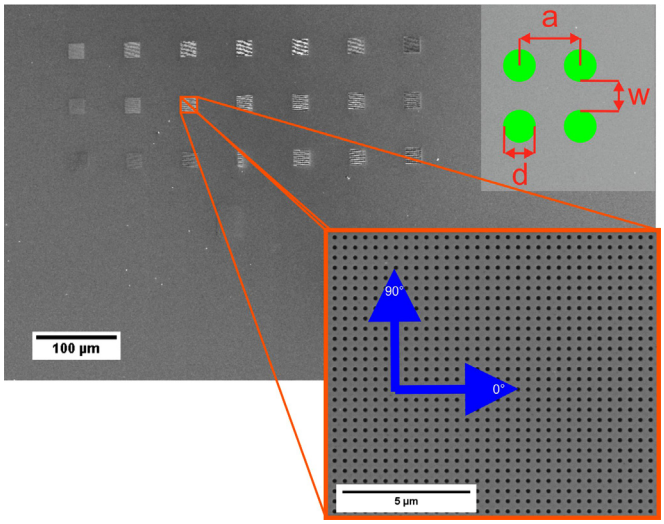

Fig. 1. Exemplary SEM image of the nano-patterned magnetic thin film with 21 different antidot lattice structures and enlargement of the antidot lattice with hole spacing $a=400$ nm and diameter $d=150$ nm.

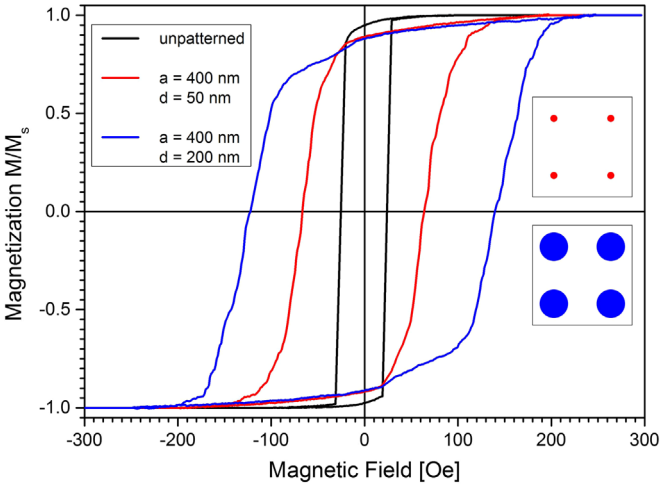

Fig. 2. Exemplary set of hysteresis loops of a pristine 20 nm Fe thin film and two square antidot lattices with different lattice parameters. The coercivity of the Fe thin film of 24 Oe increases to 65 Oe in an antidot lattice with small holes ($a=400$ nm and $d=50$ nm). The coercivity further increases to 130 Oe for an antidot lattice with larger holes ($a=400$ nm and $d=200$ nm).

drastic increase of coercivity through the nano-structuring is apparent.

The intrinsic anisotropies of the unstructured magnetic thin films, which are shown in Fig. 3, are completely suppressed in the antidot lattice, because the coercivity is increased beyond any value that occurs in the native films. Hence, measurements were taken along the 0° and 90° directions of the antidot lattices, as indicated in Fig. 1, and both values were taken into account for subsequent analysis.

3. Results and discussion

The resulting coercivities of each antidot lattice are shown in Fig. 4 as function of their respective bridge width $w = a - d$. In previous studies [12–19] a small number of antidot lattices in a narrow range has been analyzed and a simple $1/w$ relation could be fitted to the data. In our more extensive dataset, however, it was not possible to achieve an acceptable fit of the coercivity by using a $1/w$ relationship. This is exemplarily shown for Fe in Fig. 4

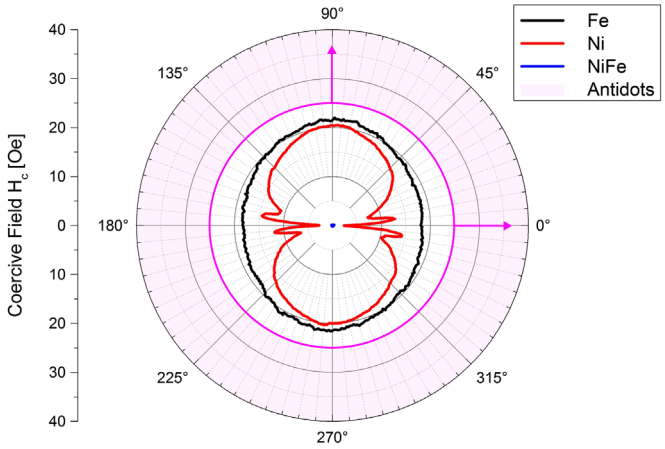

Fig. 3. Angle dependent coercivity of the pristine thin films and lower end of the coercivity range of the antidot lattices. While Fe is in-plane isotropic, the Ni thin film features an in-plane anisotropy. The coercivity of NiFe is so small that it only manifest as an isotropic point in the center of the diagram. For all antidot lattices the coercivity is larger than in the unstructured material. Thus, the anisotropies of the pristine films are not relevant in the nano-structured areas.

(a). Furthermore, Castán-Guerrero et al. [21] proposed to use an effective bridge width w_{eff} to account for material damage around the holes using five data points for antidot lattices . Indeed, accounting for a damaged area w_{damage} by assuming $w_{\mathrm{eff}} = w - w_{\mathrm{damage}}$ and a $1/w_{\mathrm{eff}}$ dependency can numerically describe our experimental data. However, the resulting fit parameters are not physically meaningful as a negative damaged area would be required to describe the NiFe data.

As the strict $1/w$ model is derived from long flat wires, it does not take the pinning efficiency of the constriction into account [22]. This cannot be directly transferred to antidot lattices as the holes are not always larger than the domain wall width. Therefore, we extended the model with a non-integer exponent of w to:

$$H_c\left(w\right) = H_c^0 + D^{oe}\cdot\frac{1}{w^p} \tag{1}$$

where H_c is the coercive field, H_c^0 is the coercive field of the unstructured film, D^{oe} is the scaling factor of the observed coercivity enhancement, and p is a non-integer exponent as model parameter. By using two model parameters both the strength and the efficiency of the domain wall pinning can be addressed. The parameters obtained from fitting the coercivity data to Eq. (1) are listed in Table 1 and the best fits are shown as dashed lines in Fig. 4. Globally an coefficient of determination R^2 value of 0.9 was calculated, indicating an acceptable fit of the data to our suggested model.

When comparing the domain wall energies [23] γ_B, that are listed in Table 1, and D^{oe} there is a similar trend in both. D^{oe}_{Fe} is one order of magnitude larger than D^{oe}_{Ni} that is in turn one order of magnitude larger than D^{oe}_{NiFe}. The ratio of D^{oe}_{Ni} and D^{oe}_{Fe} compares quantitatively to the ratio of their respective domain wall energies at 0.14 and 0.18 respectively. This strong impact of the domain wall energy on D^{oe} is to be expected, because the reduction of the domain wall length between two holes is the main source of domain wall pinning in antidot lattices [24,25]. In turn this strong domain wall pinning leads to an increase of coercivity. However, as the scaling factor D^{oe} depends on the exponent p in this model, it is not a direct measure of the domain wall energy. This is also evident from the fact that D^{oe}_{NiFe} is in comparison much smaller than would be expected from the domain wall energies alone.

Both p and, to some extent, D^{oe} are a measure of the capability of the bridges in the antidot lattice to stabilize a shortened domain

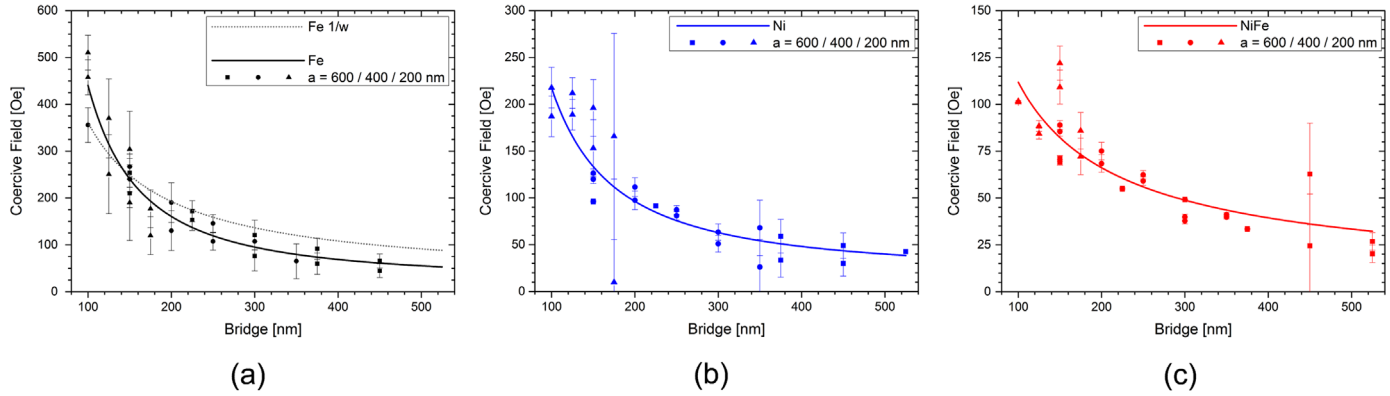

Fig. 4. Coercivities of the antidot lattices in (*a*) Fe, (*b*) Ni, and (*c*) NiFe depending on the bridge width $w = a - d$. The different symbols indicate the different lattice constants *a*. The best fits according to Eq. (1) are shown as solid lines. Additionally, for Fe a best fit for a strict $1/w$ relationship is shown as gray dotted line for comparison.

Table 1
Parameters of the best fits of the measurements shown in Fig. 4 according to Eq. (1) for Fe, Ni, and NiFe. Additionally, domain wall energies γ_B and exchange lengths l_{ex} from Kronmüller [23] are shown for comparison.

	Fe	Ni	NiFe
H_c^0 (Oe)	23.85	16.4	1.1
D^{oe} (Oe nm^{-p})	$(7 \pm 3)\cdot 10^5$	$(9 \pm 8)\cdot 10^4$	$(4 \pm 4)\cdot 10^3$
p	1.6 ± 0.1	1.3 ± 0.2	0.8 ± 0.2
γ_B (mJ m^2) $= 2\cdot\sqrt{A\cdot K_1}$ [23]	2.1	0.39	0.058
l_{ex} (nm) $= \sqrt{\frac{A}{K_1}}$ [23]	21	42	240

wall in-between two adjacent holes. Thus, indicating these constrictions are less efficient pinning centers in the case of NiFe. Considering the exchange lengths [23] l_{ex} that are listed in Table 1, it becomes evident that an assumption that the holes are larger than the domain wall width does not hold for all materials. In the case of NiFe the exchange length l_{ex} is much larger than for Fe and Ni, and for some antidot lattices even larger than the diameter *d* of the holes that are supposed to act as pinning centers for the domain walls. Thus, making a reduction of *p* plausible as the antidots do not act as efficient pinning sites and cannot drive up the coercivity in NiFe as strongly as in Fe or Ni. Because the pinning centers in an antidot lattice are circular holes, the width and the length of the material bridge between two antidots does not scale independently. Thus, the pinning strength and the domain wall length enforced by this artificial lattice of pinning sites are not independent. Additionally, considering previous work by others [22,26] on antidot lattices and thin wires it is to be expected that a dependency of D^{oe} and *p* on the film thickness may exist. While the introduction of *p* in Eq. (1) allows to account for varying pinning efficiencies of antidot lattices in different materials and a physical basis of D^{oe} and *p* can be found, an ab initio calculation from micromagnetic properties is not possible, because their mutual dependence on these properties is complex and additional influences are likely.

4. Conclusion

In summary, we have measured antidot lattices with 21 different geometries in 3 magnetic thin films to gain a broad data basis for modeling of the coercivity scaling in these nano-structured systems. By extending previous models and allowing the best fit to deviate from a $1/w$ law, we were able to model the coercivity enhancement in Fe, Ni, and NiFe and to provide a physical basis for the model parameters. The coercivity increase depends both on the domain wall energy through the reduction of the domain wall length when pinned between two holes, and the exchange length being sufficiently short in comparison to the hole diameter to allow for efficient pinning.

Acknowledgment

The authors would like to thank Bernd Ludescher for thin film deposition. Furthermore, we are grateful to Ulrike Eigenthaler for performing excellent FIB structuring and SEM measurements. Financial support by the Baden-Württemberg Stiftung within the Kompetenznetz Funktionelle Nanostrukturen is gratefully acknowledged.

References

[1] F. Haering, U. Wiedwald, T. Häberle, L. Han, A. Plettl, B. Koslowski, P. Ziemann, Geometry-induced spin-ice structures prepared by self-organization on the nanoscale, Nanotechnology 24 (2013) 055305.
[2] M.F. Laguna, C.A. Balseiro, D. Domínguez, F. Nori, Vortex structure and dynamics in kagomé and triangular pinning potentials, Phys. Rev. B 64 (2001) 104505.
[3] E. Mengotti, L.J. Heyderman, A.F. Rodriguez, F. Nolting, R.V. Hügli, H.B. Braun, Real-space observation of emergent magnetic monopoles and associated dirac strings in artificial kagome spin ice, Nat. Phys. 7 (2011) 68–74.
[4] B. Lenk, H. Ulrichs, F. Garbs, M. Münzenberg, The building blocks of magnonics, Phys. Rep. 507 (2011) 107–136.
[5] R.P. Cowburn, A.O. Adeyeye, J.A.C. Bland, Magnetic domain formation in lithographically defined antidot permalloy arrays, Appl. Phys. Lett. 70 (1997) 2309–2311.
[6] F.J. Castano, K. Nielsch, C.A. Ross, J.W.A. Robinson, R. Krishnan, Anisotropy and magnetotransport in ordered magnetic antidot arrays, Appl. Phys. Lett. 85 (2004) 2872–2874.
[7] C.C. Wang, A.O. Adeyeye, N. Singh, Magnetic antidot nanostructures: effect of lattice geometry, Nanotechnology 17 (2006) 1629–1636.
[8] F. Haering, U. Wiedwald, S. Nothelfer, B. Koslowski, P. Ziemann, L. Lechner, A. Wallucks, K. Lebecki, U. Nowak, J. Gräfe, E. Goering, G. Schütz, Switching modes in easy and hard axis magnetic reversal in a self-assembled antidot array, Nanotechnology 24 (2013) 465709.
[9] C.C. Wang, A.O. Adeyeye, Y.H. Wu, Magnetic properties of asymmetric antirectangular ni80fe20 arrays, J. Appl. Phys. 94 (2003) 6644–6648.
[10] L.J. Heyderman, F. Nolting, D. Backes, S. Czekaj, L. Lopez-Diaz, M. Kläui, U. Rüdiger, C.A.F. Vaz, J.A.C. Bland, R.J. Matelon, U.G. Volkmann, P. Fischer, Magnetization reversal in cobalt antidot arrays, Phys. Rev. B 73 (2006) 214429.
[11] G. Ctistis, E. Papaioannou, P. Patoka, J. Gutek, P. Fumagalli, M. Giersig, Optical and magnetic properties of hexagonal arrays of subwavelength holes in optically thin cobalt films, Nano Lett. 9 (2009) 1–6.
[12] I. Ruiz-Feal, L. Lopez-Diaz, A. Hirohata, J. Rothman, C.M. Guertler, J.A.C. Bland, L.M. Garcia, J.M. Torres, J. Bartolome, F. Bartolome, M. Natali, D. Decanini, Y. Chen, Geometric coercivity scaling in magnetic thin film antidot arrays, J. Magn. Magn. Mater. 242–245 (Part 1) (2002) 597–600.
[13] J.M. Torres Bruna, J. Bartolomé, L.M. García Vinuesa, F. Garcia Sanchez, J.

M. Gonzalez, O.A. Chubykalo-Fesenko, A micromagnetic study of the hysteretic behavior of antidot fe films, J. Magn. Magn. Mater. 290–291 (Part 1) (2005) 149–152.
[14] P. Prieto, K.R. Pirota, M. Vazquez, J.M. Sanz, Fabrication and magnetic characterization of permalloy antidot arrays, Phys. Status Solidi (a) 205 (2008) 363–367.
[15] K.R. Pirota, P. Prieto, A.M.J. Neto, J.M. Sanz, M. Knobel, M. Vazquez, Coercive field behavior of permalloy antidot arrays based on self-assembled template fabrication, J. Magn. Magn. Mater. 320 (2008) e235–e238.
[16] M. Vázquez, K.R. Pirota, D. Navas, A. Asenjo, M. Hernández-Vélez, P. Prieto, J. M. Sanz, Ordered magnetic nanohole and antidot arrays prepared through replication from anodic alumina templates, J. Magn. Magn. Mater. 320 (2008) 1978–1983.
[17] C. Castán-Guerrero, J. Sesé, J. Bartolomé, F. Bartolomé, J. Herrero-Albillos, F. Kronast, P. Strichovanec, K.J. Merazzo, M. Vázquez, P. Vavassori, L.M. García, Fabrication and magnetic characterization of cobalt antidot arrays: effect of the surrounding continuous film, J. Nanosci. Nanotechnol. 12 (2012) 7437–7441.
[18] E. Paz, F. Cebollada, F.J. Palomares, J.M. González, M.-Y. Im, P. Fischer, Scaling of the coercivity with the geometrical parameters in epitaxial fe antidot arrays, J. Appl. Phys. 111 (2012) 073908.
[19] C. Castán-Guerrero, J. Bartolomé, F. Bartolomé, L.M. García, J. Sesé, P. Strichovanec, J. Herrero-Albillos, K.J. Merazzo, M. Vázquez, P. Vavassori, Coercivity dependence on periodicity of co and py antidot arrays, J. Korean Phys. Soc. 62 (2013) 1521–1524.
[20] H.R. Hilzinger, H. Kronmüller, Statistical theory of the pinning of bloch walls by randomly distributed defects, J. Magn. Magn. Mater. 2 (1975) 11–17.
[21] C. Castán-Guerrero, J. Herrero-Albillos, J. Bartolomé, F. Bartolomé, L. A. Rodríguez, C. Magén, F. Kronast, P. Gawronski, O. Chubykalo-Fesenko, K. J. Merazzo, P. Vavassori, P. Strichovanec, J. Sesé, L.M. García, Magnetic antidot to dot crossover in co and py nanopatterned thin films, Phys. Rev. B 89 (14) (2014) 144405.
[22] A.O. Adeyeye, J.A.C. Bland, C. Daboo, Magnetic and magneto-transport behavior in variable width Ni80Fe20 flat wires, J. Magn. Magn. Mater. 188 (1–2) (1998) L1–L7.
[23] H. Kronmüller, S. Parkin (Eds.), Handbook of Magnetism and Advanced Magnetic Materials, Vol. 2: Micromagnetism, 2007, John Wiley & Sons, Ltd., New York, ISBN: 978-0-470-02217-7.
[24] J. Gräfe, M. Weigand, C. Stahl, N. Träger, M. Kopp, G. Schütz, E.J. Goering, Combined first-order reversal curve and x-ray microscopy investigation of magnetization reversal mechanisms in hexagonal antidot lattices, Phys. Rev. B 93 (2016) 014406.
[25] J. Gräfe, M. Weigand, N. Träger, G. Schütz, E. J. Goering, M. Skripnik, U. Nowak, F. Haering, P. Ziemann, U. Wiedwald, Geometric control of the magnetization reversal in antidot lattices with perpendicular magnetic anisotropy, Phys. Rev. B 93, 2016, 104421.
[26] K.J. Merazzo, R.P. del Real, A. Asenjo, M. Vázquez, Dependence of magnetization process on thickness of permalloy antidot arrays, J. Appl. Phys. 109 (7) (2011) 07B906.